Acta Cryst. (1992). A**48**, 545-554

The Electronic Charge Distribution in Crystalline Silicon: Comparison of *Ab Initio* Theory and Experiment

BY Z. W. LU AND ALEX ZUNGER

National Renewable Energy Laboratory, Golden, CO 80401, *USA*

(*Received* 12 *December* 1991; *accepted* 7 *February*, 1992)

Abstract

Recent consolidation by Cummings & Hart [*Aust. J. Phys.* (1988), **41**, 423-431] of five measured data sets of high-precision Si structure factors and subsequent analysis by Deutsch [*Phys. Lett. A* (1991), **153**, 368-372] produced information on the charge density of Si with precision that is unmatched by any other system. A detailed comparison with newly performed *ab initio* electronic structure calculation within the local density formalism (LDF) is presented here. The convergence of the calculation is extended to the limit at which the results reflect the predictions of the underlying LDF, unobscured by computational uncertainties. Excellent agreement (*e.g.* $R = 0.21\%$ which is three to five times better than previous calculations) is found. This allows the effects of high-index structure factors to be assessed (currently beyond the reach of high-precision measurements) on both static and dynamic deformation charge densities.

Introduction

At least 18 structure factors of Si are now known to millielectron level of accuracy, 'better by one or more order of magnitude than any other crystal' (Deutsch, 1992). Such unprecedented levels of accuracy in the structure factors and in the ensuing static electron density maps reflect both the application of precise *Pendellösung*-fringe techniques to large nearly strain-free Si single crystals and to recent careful data analysis by Spackman (1986), Cummings & Hart (1988) and Deutsch (1991, 1992). Cummings & Hart (1988) have recently consolidated five data sets obtained in three independent experiments, (Aldred & Hart, 1973; Teworte & Bonse, 1984; Saka & Kato, 1986), examining carefully the internal consistencies after corrections for anomalous dispersion (using measured wavelength-dependent f') and nuclear scattering. Very recently, Deutsch (1991, 1992) has fitted the consolidated set of $F_{\rm exp}(\mathbf{G})$ to a parametrized model density, extracting both static valence density $\rho_v(\mathbf{r})$ and deformation density $\Delta\rho(\mathbf{r})$ maps.

These recent developments have encouraged us to take a second look at the theoretically calculated structure factors and density maps of Si. There are a number of reasons for this effort. First, previous calculations were published before or during the co tion of the analysis of these high-precision Si Second, none of the previous theoretical calcul have published both an extended set of stru factors and $\rho_v(\mathbf{r})$ and $\Delta\rho(\mathbf{r})$ maps. Third, many previous calculations involved computational physical approximations that have since be unnecessary. For example, both emp pseudopotential studies (Walter & Cohen, Bertoni, Bortolani, Calandra & Nizzoli, Chelikowsky & Cohen, 1974; Baldereschi, Mas Milchev, Pickenhain & Unger, 1981) and first- ciples pseudopotential work (Haman, 1979; Z & Cohen, 1979; Zunger, 1980; Ihm & Cohen, Yin & Cohen, 1982, 1983) remove the nodal stru of the valence wavefunctions and neglect core c butions to the density. The first approxim removes the large peaks near the atomic site denced in the experimentally deduced $\rho_v(\mathbf{r})$ map Fig. 3 of Deutsch, 1991) while the second appro tion eliminates the oscillations evident in the d mation charge density (see, for example, Fi below). While the second approximation coul partially circumvented by adding the core stru factors to the pseudo-valence structure factors procedure ignores core-valence orthogonality leads to systematic errors noted by Spackman (1 All-electron calculations, which treat core valence wavefunctions on equal footing (Ra Euwema, Stukel & Collins, 1970; Stukel & Euw 1970; Wang & Klein, 1981; Dovesi, Caus Angonoa, 1981; Heaton & Lafon, 1981; Wey 1988; Methfessel, Rodriguez & Andersen, 1989; atoglou & Methfessel, 1990), are free from such plications. However, some of them involve inde dent approximations such as perturbation th (Bertoni *et al.*, 1973) or the use of small basis (Dovesi *et al.*, 1981; Heaton & Lafon, 1981). Re developments in understanding correlation effec the density functional theory (Ceperley & A 1980; Perdew & Zunger, 1981) and in nume strategies (see, for example, Wei & Krakauer, 1 Bernard & Zunger, 1989) now make highly pr calculations on simple crystals straightforward.

The basic hallmark of the calculations repo here, using the linearized augmented plane (LAPW) implementation (Wei & Krakauer, 198

Table 1. *Dynamic* (F) *and static* (ρ) *structure factors for* Si *in units of* e (atom)$^{-1}$

The experimental data (corrected for anomalous dispersion and nuclear scattering), including the estimated standard deviations σ [in me (atom)$^{-1}$] are from Cummings & Hart (1988) except the 222 reflection (Alkire, Yelon & Schneider, 1982). The difference δF_1 is $F_{calc}(\mathbf{G}) - F_{exp}(\mathbf{G})$, while $\delta F_2 = F_{sup}(\mathbf{G}) - F_{exp}(\mathbf{G})$. The root-mean-square deviation for δF_1 is 12 me (atom)$^{-1}$. The static $\rho_{exp}(\mathbf{G})$ is extracted from $F_{exp}(\mathbf{G})$ using $B = 0.4632$ Å^2 (Spackman, 1986).

	Dynamic, solid				Dynamic, atoms		Static, solid	
hkl	$F_{calc}(\mathbf{G})$ [(10)]	$F_{exp}(\mathbf{G})$ [(1)]	σ	δF_1	$F_{sup}(\mathbf{G})$ [(13)]	δF_2	$\rho_{calc}(\mathbf{G})$ [(7)]	$\rho_{exp}(\mathbf{G})$ [(2)]
111	10.600	10.6025	2.9	−3	10.455	−148	10.726	10.7281
220	8.397	8.3881	2.2	9	8.450	62	8.665	8.6557
311	7.694	7.6814	1.9	13	7.814	133	8.033	8.0204
222	0.161	0.1820	1.0	−21	0.000	−182	0.168	0.1908
400	6.998	6.9958	1.2	2	7.033	37	7.452	7.4493
331	6.706	6.7264	2.0	−20	6.646	−80	7.225	7.2473
422	6.094	6.1123	2.2	−18	6.077	−35	6.696	6.7162
333	5.760	5.7806	2.1	−21	5.769	−12	6.404	6.4270
511	5.781	5.7906	2.7	−10	5.769	−22	6.428	6.4381
440	5.318	5.3324	2.0	−14	5.302	−30	6.030	6.0462
444	4.115	4.1239	1.8	−9	4.107	−17	4.968	4.9791
551	3.931	3.9349	3.4	−4	3.925	−10	4.802	4.8072
642	3.649	3.6558	5.4	−7	3.644	−12	4.546	4.5548
800	3.253	3.2485	3.4	5	3.251	3	4.182	4.1764
660	2.917	2.9143	1.6	3	2.915	1	3.870	3.8663
555	2.802	2.8009	2.1	1	2.802	1	3.761	3.7599
844	2.165	2.1506	2.4	14	2.163	12	3.155	3.1350
880	1.543	1.5325	2.6	11	1.542	10	2.551	2.5331

the local density theory (Kohn & Sham, 1965) are as follows. (i) Core and valence wavefunctions are treated on equal footing, avoiding the pseudopotential approximation. (ii) An accurate electron-gas correlation functional (Ceperley & Alder, 1980; Perdew & Zunger, 1981) is used. (iii) No 'shape approximation' (*e.g.* muffin tin) to the potential or charge density is invoked. (iv) The basis set consists of a mix between plane waves and localized real-space functions obtained from a numerical integration of the Schrödinger equation of crystal-bound atoms. Simple (*e.g.* Slater or Gauss) orbitals are avoided. (v) The calculation is relativistic and fully self-consistent. (vi) We use an 'overkill' set of convergence parameters (size of basis set, sampling of the Brillouin zone *etc.*) so that the results reflect the underlying prediction of the Hamiltonian used (local density) rather than computational uncertainties. Our primary objective is therefore to compare the consolidated set of measured structure factors $F_{exp}(\mathbf{G})$ (Table 1), as well as the experimentally deduced valence density and density deformation maps (Deutsch, 1991, 1992) with the ultimate predictions of the local density formalism, unobscured by computational uncertainties. We have, however, a number of additional objectives, best described after the main measured and calculated quantities are defined.

Measured quantities and their modeling

We will consistently denote dynamic and static charge densities by F and ρ, respectively. Dawson (1967) has shown that if the rigid-atom approximation is invoked, the dynamic structure factor $F_{exp}(\mathbf{G})$ for momentum $\mathbf{G} = (2\pi/a)(hkl)$ can be represented as a convolution of the αth-site static structure factor $\rho_\alpha(\mathbf{G})$ and the αth-site dynamic smearing function $T_\alpha(\mathbf{G})$ as

$$F_{exp}(\mathbf{G}) = \sum_{\alpha=1}^{M} \rho_\alpha(\mathbf{G}) T_\alpha(\mathbf{G}) \exp(i\mathbf{G}\cdot\boldsymbol{\tau}_\alpha), \quad (1)$$

where $\boldsymbol{\tau}_\alpha$ is the position vector of any of the M atomic sites in the unit cell. This expression involves two universally used approximations: first, it partitions the total distribution into a linear superposition from scattering objects located at sites $\boldsymbol{\tau}_\alpha$, and second it regards each term in the superposition as a product of a term associated with a non-vibrating object positioned exactly at site α with a term that 'smears' this sharply defined position over space (Dawson, 1969). Tables 1 and 2 show the data for Si. Using the convolution approximation (1), one can extract the static structure factors

$$\rho_{exp}(\mathbf{G}) = \sum_{\alpha=1}^{M} \rho_\alpha(\mathbf{G}) \exp(i\mathbf{G}\cdot\boldsymbol{\tau}_\alpha), \quad (2)$$

e.g. by the method outlined by Dawson (1967) and refined by Stewart (1973, 1976), Coppens *et al.* (1979) and Deutsch (1991, 1992). The approach is based on the fact that any ground-state crystalline properties such as $\rho_\alpha(\mathbf{r})$ can be rigorously expanded in an infinite set of orthonormal Kubic harmonics $K_l^{a_1}(\hat{\mathbf{r}})$ of angular momentum l belonging to the totally symmetric (a_1) representation of the αth-site group

$$\rho_\alpha(\mathbf{r}) = \sum_{l=0}^{\infty} R_l(r) K_l^{a_1}(\hat{\mathbf{r}}). \quad (3)$$

Here r and $\hat{\mathbf{r}}$ are the modulus and direction, respectively, of $\mathbf{r}$ and $R_l(r)$ are radial functions for an atom

Table 2. *Dynamic* (F) *structure factors for* Si *in units of* e (atom)$^{-1}$

The experimental data (corrected for anomalous dispersion and nuclear scattering according to Cummings & Hart, 1988) are the values of Saka & Kato (1986) that were not included in the consolidated set of Cummings & Hart (Table 1). The difference δF_1 is $F_{calc}(\mathbf{G}) - F_{exp}(\mathbf{G})$, while $\delta F_2 = F_{sup}(\mathbf{G}) - F_{exp}(\mathbf{G})$. The root-mean-square deviation for δF_1 is 7 me (atom)$^{-1}$.

	Dynamic, solid			Dynamic, atom	
hkl	$F_{calc}(\mathbf{G})$ [(13)]	$F_{exp}(\mathbf{G})$ [(1)]	δF_1	$F_{sup}(\mathbf{G})$ [(1)]	δF_2
531	5.054	5.0655	−10	5.046	−20
620	4.662	4.6707	−9	4.654	−17
533	4.451	4.4552	−4	4.438	−17
711	3.929	3.9282	1	3.925	−3
553	3.494	3.5055	−12	3.489	−17
731	3.493	3.4919	1	3.489	−3
733	3.122	3.1270	−5	3.119	−8
822	2.917	2.9111	6	2.915	4
751	2.804	2.8006	3	2.802	1
840	2.628	2.6200	8	2.627	7
753	2.529	2.5274	2	2.529	2
911	2.530	2.5325	−3	2.529	−4
664	2.380	2.3677	12	2.378	10

of type α defined by the convolution of the exact $\rho_\alpha(\mathbf{r})$ with $K_l^{a_1}(\hat{\mathbf{r}})$ (we suppress the index α from R_l). For T_d symmetry, the allowed l values are $l = 0$, 3, 4, 6, 7, 8, ... ($l = 0$ is often referred to as the 'spherical term', l odd is termed the 'antisymmetric term' and l even is the 'centrosymmetric term'). Dawson's method consists of truncating (3) to include only the leading terms $l = 0$, 3 and 4 and suggesting convenient analytic guesses for the atom-localized radial functions $R_l(r)$. Deutsch used

$$R_{l=0}(r) = 4\pi \sum_{nl} \kappa_{nl}^3 \rho_{nl}(\kappa_{nl} r) \qquad (4a)$$

for the spherical term and

$$R_{l=3,4}(r) = A_l r^4 \exp(-\alpha r) \qquad (4b)$$

for the antisymmetric and centrosymmetric terms. Here κ_{nl}, A_l and α are adjustable parameters and ρ_{nl} are ground-state atomic Hartree–Fock charge densities for orbital nl (taken from Clementi, 1965). He further parametrized $T_\alpha(\mathbf{G})$ of (1) in terms of the Debye–Waller factor B_{nl} for shell nl and the anharmonic coupling factor β. Inserting into (1) the Fourier transform of the model density [(3) and (4)] and the model dynamic factor $T_\alpha(\mathbf{G})$ then gives an analytic Fourier-space representation of $F_{model}(\mathbf{G})$ in terms of $\{\kappa_{nl}, A_l, \alpha, B_{nl}, \beta\}$. The set $\{F_{model}(\mathbf{G})\}$ was then least-squares fitted to the set $\{F_{exp}(\mathbf{G})\}$ of Cummings & Hart (1988). [Note that this approach to the deconvolution of ρ and T from F is different from the 'standard spherical model' (Dawson, 1969) in which the $l \neq 0$ terms are neglected during the fit.] The best fit ('model p') produced a remarkably low R factor of 0.036% and goodness-of-fit of 1.20. The best-fit parameters were then used to calculate the model static charge density

$$\rho_{model}(\mathbf{r}) = \sum_{\mathbf{R}_i}^{\infty} \sum_{l=0,3,4} R_l|\mathbf{r} - \mathbf{R}_i| K_l|\mathbf{r} - \mathbf{R}|,$$

where ρ_α is superposed* over lattice vectors $\mathbf{R}_i$. N that this approach for extracting $\rho(\mathbf{r})$ from a se structure factors is distinct from the direct Fou synthesis method (see, for example, Pietsch, Tsirel & Ozerov, 1986). There, after deconvoluting ρ_α from $T_\alpha(\mathbf{G})$, one constructs the truncated series

$$\rho_{exp}(\mathbf{r}, \mathbf{G}_{max}) = \sum_{\mathbf{G}}^{\mathbf{G}_{max}} \rho_{exp}(\mathbf{G}) \exp(i\mathbf{G} \cdot \mathbf{r}).$$

The result depends naturally on the cut-off mom tum $\mathbf{G}_{max}$. In contrast, the model density of contains arbitrarily large momentum compone although only a limited set of structure factors is u to determine its internal parameters. We will exam below the consequences of these differences.

Calculated quantities

While diffraction experiments produce discr Fourier components of the charge density, electro structure calculations can produce the total st density $\rho_{calc}(\mathbf{r})$ directly in coordinate space. This obtained by summing the squares of the one-electr crystalline wavefunction over all occupied ba indices i and $N_\mathbf{k}$ Brillouin-zone wavevectors enclosed within the Fermi energy ε_F

$$\rho_{calc}(\mathbf{r}) = \sum_{i,\mathbf{k}}^{\varepsilon_F} N_i(\mathbf{k}) \psi_i^*(\mathbf{k}, \mathbf{r}) \psi(\mathbf{k}, \mathbf{r}),$$

where $N_i(\mathbf{k})$ is the occupation numbers of banc The Fourier components of the static charge dens can then be computed from

$$\rho_{calc}(G) = \frac{1}{\Omega} \int \rho_{calc}(\mathbf{r}) \exp(-i\mathbf{G} \cdot \mathbf{r})\, d\mathbf{r},$$

where Ω is the unit-cell volume. To compare w the experimental static charge density m $\rho_{exp}(\mathbf{r}, \mathbf{G}_{max})$ of (6), one can then filter out all Four components above a given momentum value of $\mathbf{G}_m$ obtaining

$$\rho_{calc}(\mathbf{r}, \mathbf{G}_{max}) = \sum_{\mathbf{G}}^{\mathbf{G}_{max}} \rho_{calc}(\mathbf{G}) \exp(i\mathbf{G} \cdot \mathbf{r}).$$

Comparison with the measured $F_{exp}(\mathbf{G})$ of (requires the introduction of the temperature fact into the calculation. The obvious difficulty here

* In the original work of Deutsch (1991, 1992), the sum o lattice vectors $\mathbf{R}_i$ in (5) was inadvertently truncated to a sm number of unit cells leading to lack of convergence in ρ_{model} This was corrected in the present paper in Figs. 6(b) and 7. Al the value of α in (4) published by Deutsch (1992) was in err the correct value is 2.285. We are grateful to Dr Deutsch communicating to us the correct α value.

that while the measured structure factors [(1)] naturally represent linear contributions from atomic-centered scattering centers α, there is no unique way of partitioning the calculated three-dimensional density $\rho_{\rm calc}(\mathbf{r})$ into atomic-centered quantities. Given that any partitioning of $\rho_{\rm calc}(\mathbf{r})$ into atomic-centered quantities is arbitrary, we will choose a physically appealing (but non-unique) scheme: having calculated a unique and continuous density $\rho_{\rm calc}(\mathbf{r})$, we decompose it into the 'muffin-tin' (MT) spheres around each atom α and the remaining (interstitial) volume between them. Denoting as $\rho_\alpha^{\rm MT}(\mathbf{G})$ the Fourier transform of the charge density in the αth muffin-tin sphere and by $\rho_I(\mathbf{G})$ the Fourier transform of the interstitial (I) charge density, the calculated dynamic structure factor becomes

$$F_{\rm calc}(\mathbf{G}) = \rho_I(\mathbf{G}) \exp(-\langle B\rangle G^2/16\pi^2) + \sum_{\alpha=1}^{M} \rho_\alpha^{\rm MT}(\mathbf{G}) \exp(-B_\alpha G^2/16\pi^2), \quad (10)$$

where B_α are the measured Debye–Waller factors and $\langle B\rangle$ is their average over the different atoms in the unit cell. For monoatomic crystals such as Si, $\langle B\rangle = B$. The corresponding calculated dynamic charge density map is then

$$F_{\rm calc}(\mathbf{r}, \mathbf{G}_{\rm max}) = \sum_{\mathbf{G}}^{\mathbf{G}_{\rm max}} F_{\rm calc}(\mathbf{G}) \exp(i\mathbf{G}\cdot\mathbf{r}), \quad (11)$$

which can be compared with $F_{\rm exp}(\mathbf{r}, \mathbf{G}_{\rm max})$ constructed from (1).

Partitioning the charge density

Band structures of solids generally show a clear energy separation between 'core' and 'valence' bands. Consequently, in most cases, the sum over states $(i, \mathbf{k})$ in (7) can be separated according to $\rho_{\rm tot}(\mathbf{r}) = \rho_{\rm core}(\mathbf{r}) + \rho_{\rm val}(\mathbf{r})$. Note that both components are calculated here from the mutually orthogonal solid-state wavefunctions $\{\psi_i(\mathbf{k}, \mathbf{r})\}$, hence avoiding the ambiguity of evaluating $\rho_{\rm core}(\mathbf{r})$ from atomic orbitals and $\rho_{\rm val}(\mathbf{r})$ from crystal orbitals (Stukel & Euwema, 1970). The deformation electron density map is defined as the difference

$$\Delta\rho_\mu(\mathbf{r}, \mathbf{G}_{\rm max}) = \sum_{\mathbf{G}}^{\mathbf{G}_{\rm max}} [\rho_\mu(\mathbf{G}) - \rho_{{\rm sup},\mu}(\mathbf{G})] \exp(i\mathbf{G}\cdot\mathbf{r}), \quad (12)$$

where μ stands for 'total', 'core' or 'valence'. The reference charge density corresponds to a superposition (sup) of spherically symmetric ground-state atomic charge densities $n_\alpha(r)$, yielding the Fourier components

$$\rho_{{\rm sup},\mu}(\mathbf{G}) = \sum_{\alpha=1}^{M} n_{\alpha,\mu}(\mathbf{G}) \exp(i\mathbf{G}\cdot\boldsymbol{\tau}_\alpha). \quad (13)$$

Addition of the temperature factor to (12) leads to the dynamic deformation density map denoted $\Delta F_\mu(\mathbf{r}, \mathbf{G}_{\rm max})$.

Using the model charge density of Deutsch (1991, 1992) [(4) and (5) here], one can consistently define a deformation density map by analogy with (12) as a difference between his solid-state charge density and his ground-state atomic charge density

$$\Delta\rho_{\rm model}(\mathbf{r}) = \left[\sum_{nl} \kappa_{nl}^3 \rho_{nl}(\kappa_{nl}\mathbf{r}) + R_3K_3 + R_4K_4\right] - \sum_{nl} \rho_{nl}(\mathbf{r}). \quad (14)$$

Note, however, that Deutsch defines his 'deformation density' as the quantity

$$\Delta\rho_{\rm Deutsch}(\mathbf{r}) = R_3K_3 + R_4K_4, \quad (15)$$

i.e. subtracting deformed atomic densities from the solid-state result. We will see below that the two definitions lead to qualitatively different bonding features.

Objectives

The definitions of the previous section permit a clear statement of the objectives of this study, as follows. (i) Compare $F_{\rm exp}(\mathbf{G})$ [(1)] of Cummings & Hart (1988) to $F_{\rm calc}(\mathbf{G})$ [(7), (8) and (10)], establishing the extent to which the local-density formalism can represent the most precisely known structure factors. (ii) Compare the calculated $\rho_{\rm val}(\mathbf{r})$ to Deutsch's results (1991, 1992), examining thereby the basic bonding features of Si. (iii) Compare the calculated deformation density map $\Delta\rho_{\rm tot}(\mathbf{r}, \infty)$ [(12)] to that deduced from Deutsch's fit to the data [(14)]. Establish the source of the gross discrepancy noted by Deutsch between previous calculations of $\Delta\rho_{\rm tot}(\mathbf{r})$ and his deformation density $\Delta\rho_{\rm Deutsch}(\mathbf{r})$ [(15)]. (iv) High-momentum Fourier components of $F(\mathbf{G})$ are commonly believed to be associated with core states and are expected therefore to be unimportant in determining the main features of the deformation density maps. Nevertheless, the description of the nodal structure of valence wavefunctions could require high Fourier components. Given that it is impractical to measure the very high Fourier components accurately, we will study the extent to which the main features of the calculated valence density $\rho_{\rm val}(\mathbf{r}, \mathbf{G}_{\rm max})$ and the total deformation density map $\Delta\rho_{\rm tot}(\mathbf{r}, \mathbf{G}_{\rm max})$ [(12)] are influenced by increasing $\mathbf{G}_{\rm max}$ beyond the range currently accessible to high-precision measurements. (v) It has been previously conjectured (Zuo, Spence & O'Keeffe, 1989) that even when the high-momentum Fourier components of the static deformation density $\rho(\mathbf{G}) - \rho_{\rm sup}(\mathbf{G})$ of (12) are non-negligible, the Debye–Waller factor $\exp(-BG^2)$ will damp them. Consequently, it was suggested that high Fourier components can be neglected when the

dynamic deformation density map is considered. To test this, we will compare the static deformation map $\Delta\rho_{\rm calc}(\mathbf{r}, \mathbf{G}_{\rm max})$ [(12)] to its dynamic counterpart $\Delta F_{\rm calc}(\mathbf{r}, \mathbf{G}_{\rm max})$ for a series of cut-off momenta $\mathbf{G}_{\rm max}$. (vi) Given that the model densities of (4) and (5) contain high Fourier components while conventional Fourier representations [(9)] are truncated, we will examine the ability of the latter to reproduce the former.

Convergence of the calculations

The great care with which $F_{\rm exp}(\mathbf{G})$ have been measured and analyzed calls for an equivalent assessment of the calculated counterparts. There are five basic convergence parameters that control the precision of the LAPW solution (Wei & Krakauer, 1985) to the local density Hamiltonian: (i) the number $N_{\rm basis}$ of basis functions in which $\psi_i(\mathbf{r})$ are expanded; (ii) the number $N_{\mathbf{k}}$ of special $\mathbf{k}$ points used in the Brillouin-zone summation of (7); (iii) the maximum angular momentum $l_{\rm max}$ used in the Kubic harmonic expansion [analogous to (3)]; (iv) the radius $R_{\rm MT}$ of the atomic spheres inside which the Kubic harmonic expansion is taken; (v) the number $N_{\rm den}$ of Fourier components used to expand the charge density in the interstitial region.

Table 3 shows how $\rho_{\rm calc}(\mathbf{G})$ of (8) depends on these convergence parameters. In all cases we use the experimental lattice parameter $a = 5.4307$ Å. The table shows internal convergence to better than a millielectron (me).

Dynamic and static structure factors

Table 1 gives the experimental structure factors $F_{\rm exp}(\mathbf{G})$ from the consolidated set of Cummings & Hart (1988), the estimated (Deutsch, 1992) standard deviation σ, the calculated local-density structure factors $F_{\rm calc}(\mathbf{G})$ from (8) and (10) and the difference $\delta F_1 = F_{\rm calc}(\mathbf{G}) - F_{\rm exp}(\mathbf{G})$. While $|\delta F_1|$ exceeds $|\sigma|$, the largest $|\delta F_1|$ is 22 me and the root-mean-square (r.m.s.) deviation over 18 reflections is only 12 me. This represents the best agreement achieved to date between *ab initio* calculated structure factors and experiment. Note that for some reflections (*e.g.* 222, 331, 422 and 333), the difference between theory and experiment exceeds the stated precision of both theory (see Table 3) and experiment (see σ in Table 1). We have no explanation for this. It might reflect the limiting errors due to the current imperfect knowledge of exchange correlation or deficiencies in treating the 'observed' temperature factors, *i.e.* the use of the 'rigid-atom approximation' of (1).

Table 1 also shows the dynamic superposition structure factors $F_{\rm sup}(\mathbf{G})$ [(10) and (13)], where the atomic densities n_α are also calculated from the local-density formalism using the same exchange correlation as in the crystalline calculation. The deviat from experiment $|\delta F_2| = |F_{\rm sup}(\mathbf{G}) - F_{\rm exp}(\mathbf{G})|$ is nificantly larger than $|\delta F_1|$ for $\mathbf{G} < (440)$.

Table 3. *Summary of the convergence of the calcul static* Si *structure factors*

The rows show: the number $N_{\mathbf{k}}$ of Brillouin zone $\mathbf{k}$ points us sampling the density [(7)]; the highest angular momenta $l_{\rm max}$ in the lattice-harmonics expansion [analogous to (3)]; the ave number of LAPW basis functions $N_{\rm basis}$ per atom used in wavef tion expansion; the number $N_{\rm den}$ of symmetrized star funct used to expand the charge density and potential in the inters region; the muffin-tin radius $R_{\rm MT}$ (in Å) inside which the lat harmonics expansion is carried out. The results for the diffe reflections are then given. The first column gives the actual struc factors [in units of e (atom)$^{-1}$], while the other columns show difference [in me (atom)$^{-1}$] due to various truncations.

$N_{\mathbf{k}}$	60	10	10	10	10	1
$l_{\rm max}$	12	12	12	12	8	
$N_{\rm basis}$	370	370	110	110	110	12
$N_{\rm den}$	288	288	288	91	91	10
$R_{\rm MT}$	1.164	1.164	1.164	1.164	1.164	1.1
111	10.7258	0.7	0.3	0.3	0.3	0.
220	8.6647	0.2	−0.1	−0.1	0.0	0.
311	8.0334	0.3	−0.2	−0.2	−0.1	−0.
222	0.1682	0.1	0.2	0.2	0.2	0.
400	7.4515	0.5	−0.1	−0.1	0.0	−1.
331	7.2254	0.4	0.2	0.2	0.3	0.
880	2.5506	0.1	0.0	0.1	0.0	0.

Table 2 compares our calculated $F_{\rm calc}(\mathbf{G})$ with results $F_{\rm exp}(\mathbf{G})$ of Saka & Kato (1986) that were included by Cummings & Hart (1988) in their criti compilation. We see that the differences $|\delta F_1|$ are larger than those seen in Table 1 for the Cummin Hart set. Table 1 also compares the static struct factors $\rho_{\rm exp}(\mathbf{G})$ [obtained from $F_{\rm exp}(\mathbf{G})$ using Debye–Waller factor $B = 0.4632$ Å^2] to $\rho_{\rm calc}(\mathbf{G})$ of (giving the (unweighted) R factor $\sum||\rho_{\rm exp}| - |\rho_{\rm calc}||/\sum|\rho_{\rm exp}|$. Our value $R = 0.21\%$ is two to f times better than any previous value (see compilati by Spackman, 1986). Note in particular the impro ment over the pseudopotential results, *e.g.* Yin Cohen (1982) giving $R = 1.12\%$, Zunger (1980) yie ing $R = 1.49\%$, and Chelikowsky & Cohen (19 yielding $R = 0.77\%$.

Untruncated core, valence and total charge densiti

Having established the accuracy of the calculat $F_{\rm calc}(\mathbf{G})$ and $\rho_{\rm calc}(\mathbf{G})$ over the limited set of momer accessible to high-precision measurements, we n consider the calculated real-space charge density [(without any Fourier truncation. Fig. 1 depicts t calculated $\rho_{\rm core}(\mathbf{r})$, $\rho_{\rm val}(\mathbf{r})$ and their sum $\rho_{\rm tot}(\mathbf{r})$, wh Fig. 2 shows the corresponding deformation densiti $\Delta\rho_{\rm core}(\mathbf{r})$, $\Delta\rho_{\rm val}(\mathbf{r})$ and $\Delta\rho_{\rm tot}(\mathbf{r})$ [(12) for $\mathbf{G}_{\rm max} \to \infty$ The basic features are as follows. (i) $\rho_{\rm val}(\mathbf{r})$ h absolute maxima on the atomic sites, a bondi density oriented parallel to the bond direction wi a local minimum at the bond center and accumulati of charge at the back-bond regions (marked α

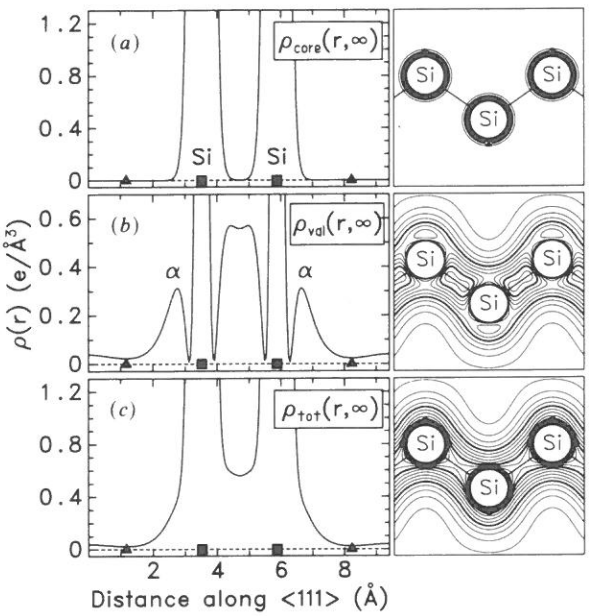

Fig. 1. Untruncated ('$\mathbf{G}\to\infty$') *ab initio* static charge densities for (*a*) core states, (*b*) valence states and (*c*) all occupied states. In this and all subsequent figures, we show side-by-side line plots in the ⟨111⟩ direction and contour plots in the (110) plane. The solid squares denote atomic positions while solid triangles denote the (empty) tetrahedral interstitial sites. Contour step = 0.05 e Å^{-3}. The outmost contour is at 0.05 e Å^{-3}.

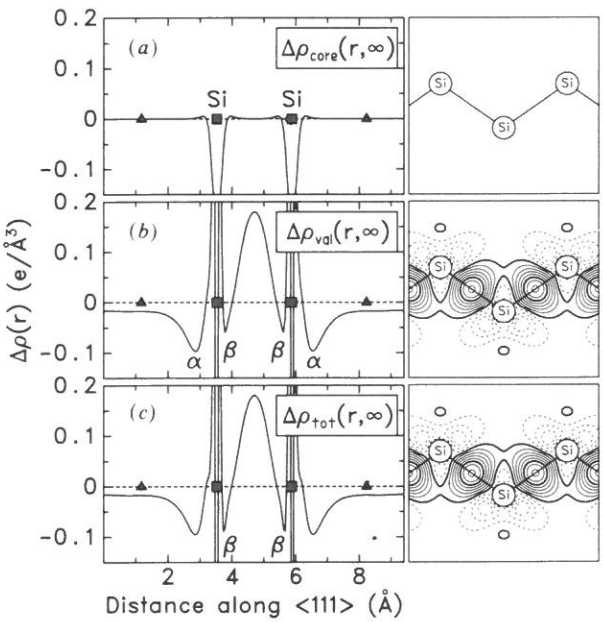

Fig. 2. Untruncated ('$\mathbf{G}\to\infty$') *ab initio* static deformation charge densities [(12)] for (*a*) core states, (*b*) valence states and (*c*) all occupied states. The thick outer solid contour next to the dashed line denotes $\Delta\rho = 0$. Contour step = 0.025 e Å^{-3}.

Fig. 1*b*). In contrast, the corresponding deformation density $\Delta\rho_{val}(\mathbf{r})$ has minima near the atomic sites, a bonding density lobe oriented perpendicular to the bond direction with a maximum at the bond center and depletion of charge from the back-bond regions α. Furthermore, the amplitude of $\Delta\rho_{val}$ at the bond center is only about a third of ρ_{val}. Clearly, many of the features of ρ_{val} are dominated by atomic characteristics. (ii) As expected, $\rho_{core}(\mathbf{r})$ is localized near the atoms so that $\Delta\rho_{core}(\mathbf{r})$ is mostly empty, with the exception of a localized charge depletion inside the atomic cores. Clearly the core is not entirely inert. Since, however, this non-inertness is highly localized in space, $\rho_{val}(\mathbf{r})$ and $\Delta\rho_{tot}(\mathbf{r})$ are very similar over most of the unit-cell space. (iii) The deformation density maps $\Delta\rho_{tot}$ and $\Delta\rho_{val}$ have sharp nodal features near the core and sharp minima in the 'inner-bond region' (point β in Fig. 2), both reflecting the fact that the nodes in the crystal valence wavefunctions are shifted with respect to those in the free-atom valence orbitals. As will be shown below, these sharp features will require relatively high momentum components in a Fourier description. These features, as well as the atom-centered maxima in $\rho_{val}(\mathbf{r})$, are missing from all pseudopotential calculations since they use nodeless pseudo-orbitals.

Fourier-truncated charge density maps

Given that even deformation charge density maps exhibit rather sharp features in **r** space, we next examine the convergence of their Fourier representation. Fig. 3 depicts the individual contributions from distinct beams $[\rho_{calc}(\mathbf{G}) - \rho_{sup}(\mathbf{G})]\exp(i\mathbf{G}\cdot\mathbf{r})$ [summands of (12)] to the total deformation charge density $\Delta\rho_{calc}(\mathbf{r})$. Each of these terms can be characterized by, for example, the sign of the amplitude on: (i) atoms, (ii) bonds and (iii) tetrahedral interstitial sites (marked as solid triangles in all line plots), respectively. For instance, the (220) contribution has the respective signs $(-, 0, -)$, the (311) beams is $(-, +, +)$, the (222) beam is $(0, +, 0)$, the (331) beam is $(+, +, -)$ *etc.* The variations in these signs with **G** suggest limited cancellations among the different $\Delta\rho(\mathbf{G})\exp(i\mathbf{G}\cdot\mathbf{r})$ values as the Fourier series is summed up over **G**. This rate of convergence is examined in more detail in Fig. 4 where we plot the calculated $\Delta\rho_{tot}(\mathbf{r}, \mathbf{G}_{max})$ of (12) for three sets of **G** vectors. First, (Fig. 4*a*) we use calculated $\rho_{calc}(\mathbf{G})$ at the set **G** vectors of Cummings & Hart (1988) (Table 1), employed also by Deutsch (1991, 1992) in his analyses. While this set extends to $\mathbf{G} \leq (880)$, it contains only 18 of the 52 allowed reflections contained in this range. Second, (Fig. 4*b*) we show $\Delta\rho_{tot}$ calculated from all reflections up to $\mathbf{G}_{max} = (880)$. Finally, (Fig. 4*c*) we depict $\Delta\rho_{tot}$ for $\mathbf{G}_{max} = (12,12,12)$, outside the range of current high-precision measurements. The latter $\Delta\rho$ plot closely resembles the untruncated

$\Delta\rho_{tot}(\mathbf{r}, \infty)$ of Fig. 2(*c*) (except for the inner core region). The evolution of $\Delta\rho_{tot}(\mathbf{r}, \mathbf{G}_{max})$ with $\mathbf{G}_{max}$ seen in Fig. 4 clearly exhibits robustness of the amplitude near the bond center. As expected, the largest difference between a smaller and a larger set of **G** vectors is visible near the atomic sites; the difference diminishes somewhat away from these sites. At the same time, the amplitude on the inner-bond minima β and back-bond minima α is far from convergence using a limited number of reflections, *i.e.* Deutsch's set.

Fig. 5 shows the evolution of $\rho_{val}(\mathbf{r}, \mathbf{G}_{max})$ with the highest value of $\mathbf{G}_{max}$ (indicated in the inserts) included in the Fourier series of the type of (9). (sees a transition from smooth behavior at low **G** (Fig. 5*a*) to an oscillatory function at intermed $\mathbf{G}_{max}$ values (Figs. 5*c*, *d*, *e*) and finally to a smc function at high $\mathbf{G}_{max}$ values (Fig. 5*f*). The la Fourier-synthesized function is nearly indistingu able from the real-space representation $\rho_{val}(\mathbf{r}, \infty$ Fig. 1(*b*). Like Fig. 4, Fig. 5 also shows that, des the high precision of the individual X-ray struc factors in the Cummings–Hart–Deutsch set, it is small to capture the full structure of the conver charge density. The best that can be done to date way of convergence of the measured series [Figs. 4 and 5(*e*)] is still rather different from the converge limit [Figs. 4(*c*) and 5(*f*), respectively].

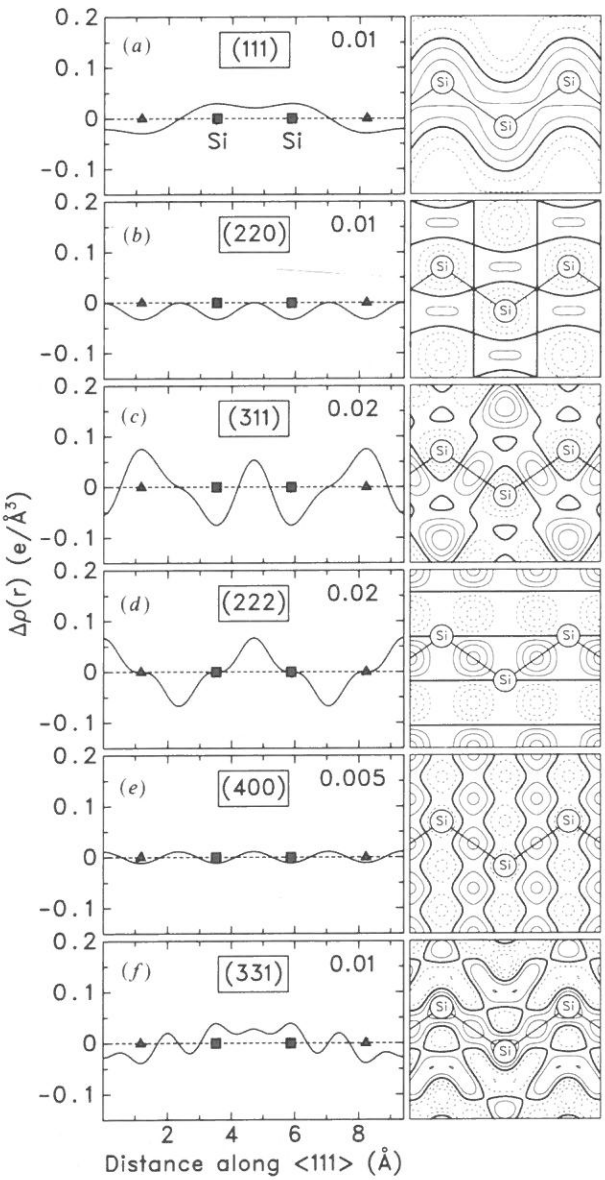

Fig. 3. Contributions of individual beams [summand of (12) for individual **G** vectors] to the total static deformation charge density. The inserts denote contour steps in e Å^{-3}.

Comparison with the model charge densities: ρ_v

The text surrounding (5) and (6) highlights the fun mental difference between a Fourier synth approach [(6), illustrated in Figs. 4 and 5] an model density approach [(5)] of Dawson (19 Stewart (1973, 1976), Coppens *et al.* (1979) Deutsch (1991, 1992): the latter method is guarante by construction, to yield a smooth function des the use of a limited set of structure factors. We hence next compare the results of the model den to our fully converged results.

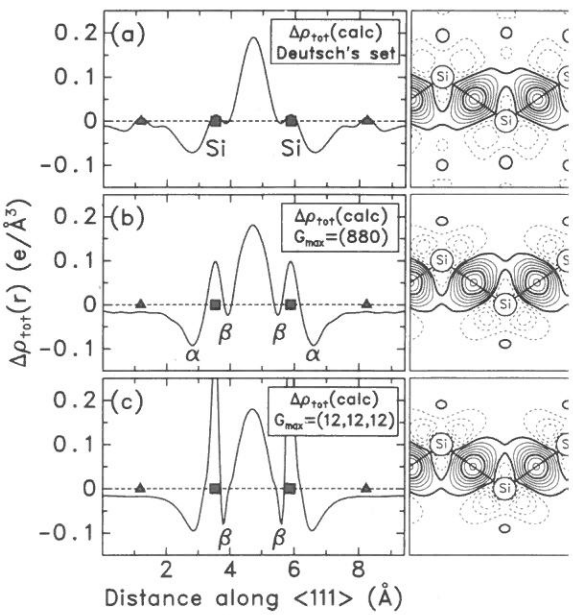

Fig. 4. Convergence of the *ab initio* calculated static deforma charge density $\Delta\rho$ [(12)] with respect to the set of reflecti included in the Fourier series: (*a*) the Cummings–Hart–Deu set of **G** vectors (Table 1); (*b*) all reflections up to $\mathbf{G}_{max} = (8$ and (*c*) all reflections up to $\mathbf{G}_{max} = (12,12,12)$. Contour ste 0.025 e Å^{-3}. Note that (*c*) is practically identical to the unti cated $\Delta\rho$ of Fig. 2(*c*).

Fig. 6 compares our calculated $\rho_{\rm val}(\mathbf{r},\infty)$ with Deutsch's model valence density [(5), where the $nl=1s, 2s, 2p$ atomic core components of $R_{l=0}(r)$ in (4) are omitted]. The agreement between theory and the experimentally derived function is very good. Quantitatively, we find amplitudes of 0.313, 0.570 and 0.577 e Å^{-3} on the back-bond maxima α, the bond-center peak and the bond-center dip, respectively, while Deutsch finds the values 0.298, 0.579 and 0.575, respectively. The crescent-shaped peak behind the atoms is 0.383 e Å^{-3}, while Deutsch's value is 0.355 e Å^{-3}. Our peak-to-saddle difference near the bond center is 13 me Å^{-3}, compared with Deutsch's value of 4 me Å^{-3}. The only significant discrepancy exists in the inner-bond minima (point β), where our results shows a significantly lower amplitude than Deutsch's fit. Fig. 4 demonstrates, however, that this feature is highly dependent on Fourier truncation, so using more reflections in Deutsch's fit could change this value. Our results and those of Deutsch are very different from the elliptic single-peaked density obtained by Yang & Coppens (1974) using a truncated Fourier series.

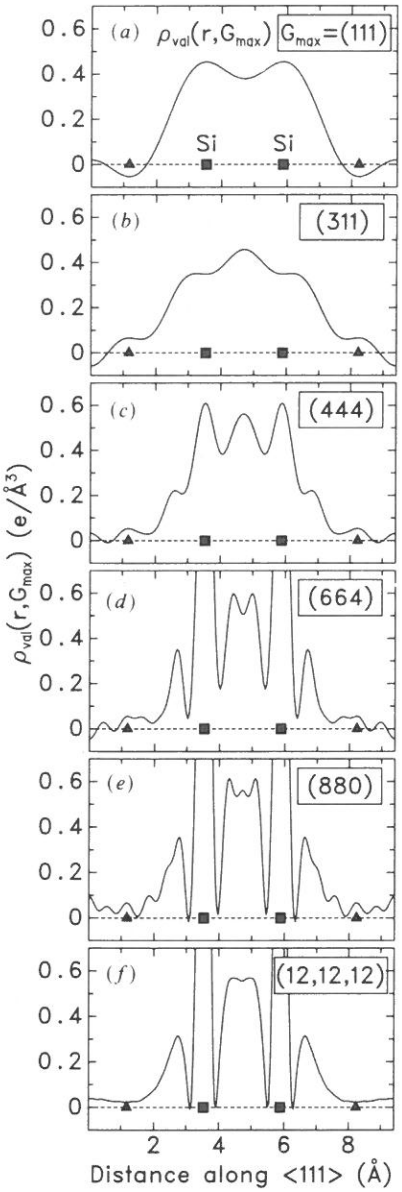

Fig. 5. Convergence of the *ab initio* calculated static valence density $\rho_{\rm val}$ with respect to the highest momentum included in the Fourier sum. Note that (*f*) is practically identical to the untruncated $\rho_{\rm val}$ of Fig. 1(*b*).

Comparison with the model charge densities: $\Delta\rho_{\rm tot}$

Fig. 7(*a*) shows the deformation density map $\Delta\rho_{\rm Deutsch}(\mathbf{r})$ as defined by Deutsch [(15)] and

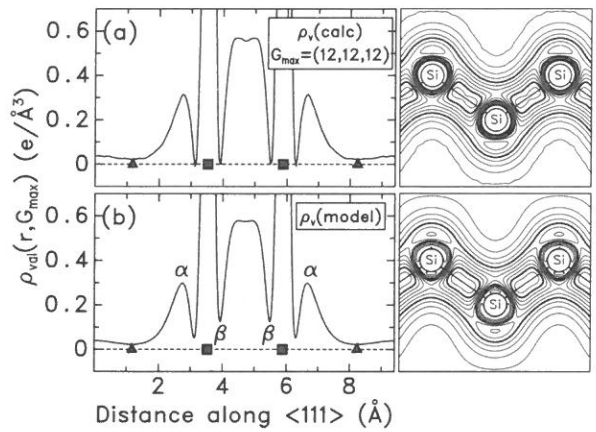

Fig. 6. Comparison of (*a*) the *ab initio* calculated static valence charge density $\rho_{\rm val}$ with (*b*) Deutsch's fit to the data of Cummings & Hart (1988). Contour step = 0.05 e Å^{-3}.

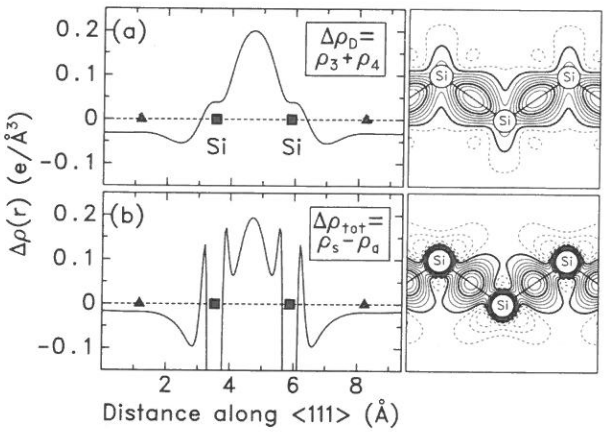

Fig. 7. Comparison of two experimentally deduced static density deformation plots: (*a*) Deutsch's definition [(15)] in which deformed atoms are used as a reference and (*b*) the conventional definition [(14)] in which ground-state atoms are used as reference. In both cases, Deutsch's parameters are used. Contour step = 0.025 e Å^{-3}.

calculated with his model parameters (fit p). This is identical to his (1991) Fig. 1. We see that $\Delta\rho_{\text{Deutsch}}(\mathbf{r})$ exhibits a bond charge density that is elongated parallel to the bond direction. On this basis, Deutsch has criticized the calculation of Wang & Klein (1981), which showed a deformation density that is elongated perpendicular to the bond direction. However, Wang & Klein used the conventional definition of deformation density, *i.e.* the difference between crystalline and ground-state atomic densities, while Deutsch's definition [(15)] subtracts deformed atomic densities from the crystalline density. Fig. 7(b) shows $\Delta\rho_{\text{model}}(\mathbf{r})$ in which Deutsch's parameters are used in conjunction with the standard definition, *i.e.* (14). We see that there is an elongation perpendicular to the bond direction, in qualitative agreement with Wang & Klein. The quantitative agreement remains, however, poor, as noted by Deutsch (1992).

Fig. 4(c) shows our *ab initio* calculated deformation charge density $\Delta\rho_{\text{tot}}$ [(12) for $\mathbf{G}\to\infty$]. Comparison with Deutsch's (corrected) model (Fig. 7b) shows quantitative agreement: $\Delta\rho_{\text{tot}}$ is perpendicular to the bond, has a bond-center maximum of 0.180 e Å^{-3} (compared with Deutsch's result of 0.194 e Å^{-3}) and a minimum at the back-bond position α (0.67 Å away from the atom) with an amplitude of 0.095 e Å^{-3} (compared with Deutsch's result of 0.096 e Å^{-3}, at 0.69 Å away from the atom). The details in the outer-bond regions β (best seen in the line plot) are, however, significantly different. Deutsch's model shows sharp peaks at the β points with pronounced minima on the atomic sites. These features are unmatched by any Fourier synthesis (Fig. 4) and reflect, in our opinion, the difficulty in reproducing the complexity of a realistic $\Delta\rho_{\text{tot}}$ within the arbitrary restricted representation for $R_l(r)$ [(4)]. It is remarkable, however, that despite the clear insufficiency of the Cummings–Hart–Deutsch set of momenta to describe ρ_{val} or $\Delta\rho_{\text{tot}}$ in a Fourier representation (see Figs. 4 and 5), the model density approach of (4) and (5) mimics very well the overall results obtained from a highly converged Fourier series.

Static *vs* dynamic deformation densities

Zuo, Spence & O'Keeffe (1989) conjectured that even if the inclusion of the high-momentum Fourier components will affect the shape of the static deformation densities $\Delta\rho(\mathbf{r}, \mathbf{G}_{\max})$, they will be inconsequential for the dynamic deformation density $\Delta F(\mathbf{r}, \mathbf{G}_{\max})$, since the Debye–Waller factors will effectively attenuate such high $\mathbf{G}$ components. To test this hypothesis, we plotted in Fig. 8 the static $\Delta\rho_{\text{tot}}$ and the dynamic ΔF_{tot} for two truncations: $\mathbf{G}_{\max}=(331)$ (Figs. 8a and b) and $\mathbf{G}_{\text{big}}=(12,12,12)$. This shows that $\Delta\rho_{\text{tot}}\cong\Delta F_{\text{tot}}$ at any of these truncations, thus invalidating the conjuncture of Zuo *et al.* Clearly, the Debye–Waller exponent $\exp(-G^2B)$ does not decay fast enough in the range where $\Delta\rho(\mathbf{G})$ is non-negligible. This impl that the difficult to calculate (by *ab initio* metho dynamic charge density can be effectively replac by the far simpler static density calculations. Al since high-momentum Fourier components $F(\mathbf{G}_{\text{b}}$ clearly affect charge density deformation plots (Figs. 4 and 8) and valence charge density plots (Fig. 5), the current inability to measure $F(\mathbf{G}_{\text{big}})$ w high precision poses a real limitation to our abil to characterize $\Delta\rho_{\text{tot}}(\mathbf{r})$ accurately by experiment.

Concluding remarks

(i) State-of-the-art local-density theory is able reproduce all accurately measured Si structure facto with a maximum error of ~20 me and often consid ably better. R factors for 18 reflections are as sm as 0.21%. (ii) The valence charge density ρ_{val}(extracted from experiment is accurately reproduc by our theory (Fig. 6). (iii) The global features of t total deformation density $\Delta\rho_{\text{tot}}(\mathbf{r})$ deduced fro experiment are reproduced well by our theory [Fig 4(c) and 7(b)]. The sharp features in the expe mentally deduced $\Delta\rho_{\text{model}}(\mathbf{r})$ are, however, u matched by theory at any level of Fourier truncatio

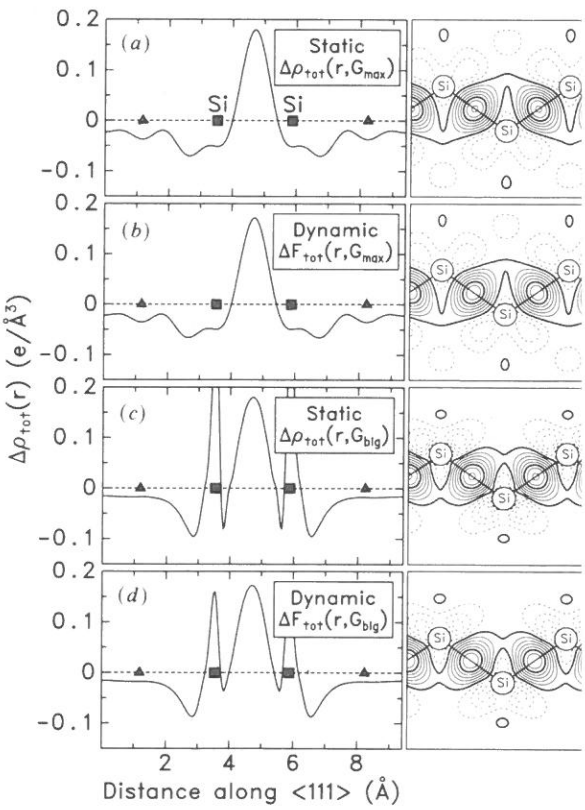

Fig. 8. Comparison of static ($\Delta\rho$) and dynamic (ΔF) densi deformation maps for two Fourier truncations: $G_{\max}=(331)$ (a) and (b) and $\mathbf{G}_{\text{big}}=(12,12,12)$ in (c) and (d). Contour step 0.025 e Å^{-3}.

We suspect that this reflects a limitation in the choice of simple radial functions [(4)] in the fit to experiment. (iv) Valence charge densities $\rho_{val}(\mathbf{r})$ and deformation charge densities $\Delta\rho_{tot}(\mathbf{r})$ exhibit some localized features reflecting changes in the atomic nodal structures by the crystalline environment [Figs. 1(*a*) and 2(*c*)]. This leads to moderately slow convergence of the respective Fourier series (Figs. 4 and 5). Even the (relatively large) set of reflections used by Cummings & Hart (1988) is insufficient for capturing such features in a Fourier synthesis. A similar situation exists for GaAs, where the measured reflections (Zuo, Spence & O'Keeffe, 1988) were shown (Bernard & Zunger, 1989) to be insufficient to capture the main features of $\Delta\rho_{tot}$. The model density approach [(3)–(5)], however, is able to reproduce the global features of a highly converged Fourier series. (v) The conjecture of Zuo, Spence & O'Keeffe (1989) that high-momentum components will not significantly modify dynamical deformation maps is not supported by our calculations. We find that the static maps $\Delta\rho(\mathbf{r}, \mathbf{G}_{max})$ closely track the dynamic maps $\Delta F(\mathbf{r}, \mathbf{G}_{max})$ for any $\mathbf{G}_{max}$. In view of (iv) above, this implies that the current inability to measure high Fourier components accurately does affect the accuracy of the ensuing deformation density maps.

As a final note we remark that the *ab initio* calculations of the type reported here are now very simple and inexpensive to carry out: starting from scratch, the Si calculation involving convergence limits that produce better than 1 me error in any $\rho(\mathbf{G})$ take only 3 min on a CRAY YMP computer and involve no human intervention. As accurate data on other crystals becomes available, similar calculations could readily be carried out.

We are grateful to M. Deutsch for stimulating discussions on the subject and to J. Spence and M. Hart for critical reading of the manuscript. This work was supported by the US Department of Energy, Office of Energy Research, Basic Energy Science, Grant DE-AC02-77-CH00178.

References

ALDRED, P. J. E. & HART, M. (1973). *Proc. R. Soc. London Ser. A*, **332**, 223–238, 239–254.

ALKIRE, R. W., YELON, W. B. & SCHNEIDER, J. R. (1982). *Phys. Rev. B*, **26**, 3097–3104.

BALDERESCHI, A., MASCHKE, K., MILCHEV, A., PICKENHAIN, R. & UNGER, K. (1981). *Phys. Status Solidi B*, **108**, 511–520.

BERNARD, J. E. & ZUNGER, A. (1989). *Phys. Rev. Lett.* **62**, 2328.

BERTONI, C. M., BORTOLANI, V., CALANDRA, C. & NIZZOLI, F. (1973). *J. Phys. C*, **6**, 3612–3630.

CEPERLEY, D. M. & ALDER, B. J. (1980). *Phys. Rev. Lett.* **45**, 566–569.

CHELIKOWSKY, J. R. & COHEN, M. L. (1974). *Phys. Rev. B*, **10**, 5095–5107.

CLEMENTI, E. (1965). *IBM J. Res. Dev.* **9**, Suppl. 2.

COPPENS, P., GURU ROW, T. N., LEUNG, P., STEVENS, E. D., BECKER, P. J. & YANG, Y. W. (1979). *Acta Cryst.* A**35**, 63–72.

CUMMINGS, S. & HART, M. (1988). *Aust. J. Phys.* **41**, 423–431.

DAWSON, B. (1967). *Proc. R. Soc. London Ser. A*, **298**, 264–288, 379–394.

DAWSON, B. (1969). *Acta. Cryst.* A**25**, 12–29.

DEUTSCH, M. (1991). *Phys. Lett. A*, **153**, 368–372.

DEUTSCH, M. (1992). *Phys. Rev. B*, **45**, 646–657.

DOVESI, R., CAUSA, M. & ANGONOA, G. (1981). *Phys. Rev. B.* **24**, 4177–4183.

HAMAN, D. R. (1979). *Phys. Rev. Lett.* **42**, 662–665.

HEATON, R. & LAFON, E. (1981). *J. Phys. C*, **14**, 347–351.

IHM, J. & COHEN, M. L. (1980). *Phys. Rev. B*, **21**, 1527–1536.

KOHN, W. & SHAM, L. J. (1965). *Phys. Rev.* **140**, A1133–A1138.

METHFESSEL, M., RODRIGUEZ, C. O. & ANDERSEN, O. K. (1989). *Phys. Rev. B*, **40**, 2009–2012.

PERDEW, J. P. & ZUNGER, A. (1981). *Phys. Rev. B*, **23**, 5048–5079.

PIETSCH, U., TSIRELSON, V. G. & OZEROV, R. P. (1986). *Phys. Status Solidi B*, **137**, 441–447.

POLATOGLOU, H. M. & METHFESSEL, M. (1990). *Phys. Rev. B*, **41**, 5898–5903.

RACCAH, P. M., EUWEMA, R. N., STUKEL, D. J. & COLLINS, T. C. (1970). *Phys. Rev. B*, **1**, 756–763.

SAKA, T. & KATO, N. (1986). *Acta Cryst.* A**42**, 469–478.

SPACKMAN, M. A. (1986). *Acta Cryst.* A**42**, 271–281.

STEWART, R. F. (1973). *J. Chem. Phys.* **58**, 1668–1676.

STEWART, R. F. (1976). *Acta Cryst.* A**32**, 565–574.

STUKEL, D. J. & EUWEMA, R. N. (1970). *Phys. Rev. B*, **1**, 1635–1643.

TEWORTE, R. & BONSE, U. (1984). *Phys. Rev. B*, **29**, 2102–2108.

WALTER, G. P. & COHEN, M. L. (1971). *Phys. Rev. B*, **4**, 1877–1892.

WANG, C. S. & KLEIN, D. M. (1981). *Phys. Rev. B*, **24**, 3393–3416.

WEI, S.-H. & KRAKAUER, H. (1985). *Phys. Rev. Lett.* **55**, 1200–1203.

WEYRICH, K. H. (1988). *Phys. Rev. B*, **37**, 10269.

YANG, Y. W. & COPPENS, P. (1974). *Solid State. Commun.* **15**, 1555–1559.

YIN, M. T. & COHEN, M. L. (1982). *Phys. Rev. B*, **26**, 5668–5687.

YIN, M. T. & COHEN, M. L. (1983). *Phys. Rev. Lett.* **50**, 1172.

ZUNGER, A. (1980). *Phys. Rev. B*, **21**, 4785–4790.

ZUNGER, A. & COHEN, M. L. (1979). *Phys. Rev. B*, **20**, 4082–4108.

ZUO, J. M., SPENCE, J. C. H. & O'KEEFFE, M. (1988). *Phys. Rev. Lett.* **61**, 353–356.

ZUO, J. M., SPENCE, J. C. H. & O'KEEFFE, M. (1989). *Phys. Rev. Lett.* **62**, 2329.